Rodríguez-Sánchez, M.R., …et al. (2014). Saving assessment using the PERS in solar power towers, *Energy Conversion and Management*, v. 87, pp.: 810-819.

DOI: https://doi.org/10.1016/j.enconman.2014.07.076

Saving assessment using the PERS in solar power towers.

M.R. Rodriguez-Sanchez[1*], A. Sanchez-Gonzalez[1], C. Marugan-Cruz[1], D. Santana[1].

[1] Energy Systems Engineering Group (ISE), Department of Fluids and Thermal Engineering, Universidad Carlos III of Madrid.

Av. Universidad 30, Leganés, 28911 Madrid (Spain)

*Phone number: +34 916246034, Fax: +34916249430, e-mail: **mrrsanch@ing.uc3m.es**

Abstract

The improvement of the solar power tower using solar salt is one of the main goals of researchers. Any method or invention to improve the efficiency of this technology contributes to promote the renewable energies. The use of a Potential Energy Recovery System (PERS) in two different solar power tower plants of 20 and 100 MW has been analysed.

The PERS is formed, at least, by one turbine, located at the hot salt pipe coming from the receiver. The turbine is engaged to the shaft of the feed pump, which raises the heat transfer fluid from the cold tank to the receiver. It reduces the parasitic power consumption of the plant, and increases its global efficiency.

Different PERS configurations have been modelled. Based on an energetic and economic analysis, the optimal configuration is a geometrical similar turbine of three times the volume flow rate of one feed pump. The PERS has been proven to be a cost reductive and clean tool. For a 100 MW power plant of 30-year lifetime the investment cost is 1.26 M$ and the annual cash flow is 0.89 M$, while for a plant of 20 MW these values are 0.26 M$ and 0.19 M$, respectively.

Key words: Solar Power Tower; Parasitic Power Consumption; Potential Energy; Storage Tanks.

Nomenclature

Abbreviations

CBA: Cost-Benefit Analysis.

DNI: Direct Normal Irradiance [W/m^2].

HTF: Heat transfer fluid.

PERS: Potential Energy Recovery System.

SPT: Solar Power Tower.

PAT: Pump As Turbine.

PPA: Power Purchase Agreement.

TNPV: Total Net Present Value.

Symbols

A : Area, Surface [m^2].

B : Benefit [$].

C : Cost [$].

C_p : Specific heat [J/kgK].

D : Diameter [m].

E : Power [W].

H : Head [Pa].

N : Number of elements [-].

P : Price [$].

Q : Volume of HTF by unit of time [m^3/h].

S : Distance from the heliostat to the tower optical height [m].

T : Temperature [K].

W : Shaft power [W].

f : Carbon dioxide released [-].

g : Gravity acceleration [m/s^2].

h : Length [m].

$\dot{m}$: Mass flow rate [kg/s].

p : Pressure [Pa].

r : Loan interest rate [-].

ref : Reflectivity [-].

t : Income tax rate [-].

x : Whole service period [year].

y : Repayment time [year].

Greek letters:

Δp : Pressure drop [Pa].

β : Angle between the solar radiation direction and the heliostat's normal [º].

η : Efficiency [-].

θ : Inflation rate [-].

ρ : Density [kg/m^3].

τ : Discount rate [-].

Subscripts

HTF : Heat transfer fluid.

I : Interest.

O : Operation and maintenance.

T : Tax.

at : Atmospheric.

c : Coal.

ci : Initial investment.

$field$: Field.

hel : Heliostat.

in : Inlet.

$\max$: Maximum.

out : Outlet.

p : Principal repaid.

$pump$: Pump.

rec : Receiver.

s : Solar electricity.

sp : Spillage.

$s\&b$: Shadow and Blocking.

tank : Tank.

$turb$: Turbine.

1. Introduction.

In recent years there is a resurgent interest in concentrating solar power technologies with storage. One of the most promising technologies is the Solar Power Tower (SPT), due to its high availability and dispatchability. Industry and laboratory research efforts are now focusing on optimizing SPT. Precisely, there are numerous SPT around the world used for research: NSTTF (New Mexico), PSA (Spain), Julich Solar Tower (Germany), CSIRO (Australia), or Thémis (France) are some examples [1–3].

The central receiver concept is based on a field of individually sun-tracking mirrors, which reflect the incident solar radiation to a receiver at the top of a tower. This way, the direct radiation is concentrated in the receiver allowing it to reach high solar flux.

Typically, 75% to 90% of the reflected energy is absorbed and transferred to a working fluid, which is pumped up the tower [4–8].

SPT usually include a cold storage tank and a hot storage tank at the bottom of the tower, which provide and collect the fluid that flows through the receiver. The heat transfer fluid (HTF) is pumped from the cold tank to the top of the tower, flowing through the receiver. And then, the hot HTF is collected in the hot tank or is sending to the evaporation train, that usually is a super-critical Rankine cycle [9]. In the receiver outlet, the HTF has high mechanical energy, sum of its kinetic energy and of its potential energy, result of the height of the tower.

Due to the high pressure at the hot tank inlet, it is necessary to laminate the flow to avoid overpressure in the hot tank and possible damages in the storage system. A passive system of plates that produces the necessary pressure drop has been traditionally employed. The energy dissipated by pressure drop is an energy sink.

In order to improve the SPT efficiency several actions have been recommended by Kolb et al [10]: optimize the heliostat field layout, optimize the receiver design [11], increase the plant availability, improve the power block, and/or improve the energy balance.

It has been proved that the electrical power required by the SPT to generate solar electricity (parasitic power) is relatively high, at least 10% of the energy produced [10]. This parasitic power consumption can be divided in the three main blocks of the SPT: the heliostat field with the tracking system, the receiver with the salt-circulation and the receiver feed pumps, and the power system with the steam-circulation, booster and condenser pumps. The only system susceptible to recover part of its consumed power is the molten salt pumps that feed the receiver. In addition, the mayor parasitic power of the plant is consumed by these pumps.

Therefore, this study is focused on the improvement of the energy balance of SPT, by means of the implementation of a system that allows the recovery of the potential energy of the hot HTF that comes from the receiver. The studied Potential Energy Recovery System (PERS) is formed at least by a turbine that substitutes the current passive system of energy dissipation, which avoids damages in the hot tank. This turbine would be connecting to the shaft of the feed pump to save a significant part of the energy used to pump the HTF to the receiver. This way, the parasitic power consumption of the thermal power plant will be reduced, improving the performance and the economic profit.

In this article two different sizes of SPT have been studied; one plant has a power forecast generation of 100 MW, and the other one of 20 MW. Both plants use molten salt as HTF. To complete the study, different PERS configurations have been analysed to find the optimal PERS design for each plant.

Firstly, the SPT studied and theirs heliostat fields have been defined. Then, the hourly mass flow rate at the receiver has been estimated by the annual solar irradiation data. The power necessary to raise the HTF to the receiver and the power recovered by the PERS can be evaluated from the intersection of the pump/turbine characteristic curve, provided by the manufacturers, and the system resistance curve, calculated from the mass flow rate at the receiver.

2. Potential Energy Recovery System (PERS) description.

The PERS is a system formed at least by a radial or an axial turbine on the hot salt pipe coming from the receiver, close to the bottom of the tower (see Figure 1). The aim of the PERS is to reduce the parasitic power consumption of SPT, recovering the potential energy from the HTF that usually is wasted, and then increasing the energy balance of the SPT. The PERS can be used in SPT working with different HTF, except for those with direct steam generation.

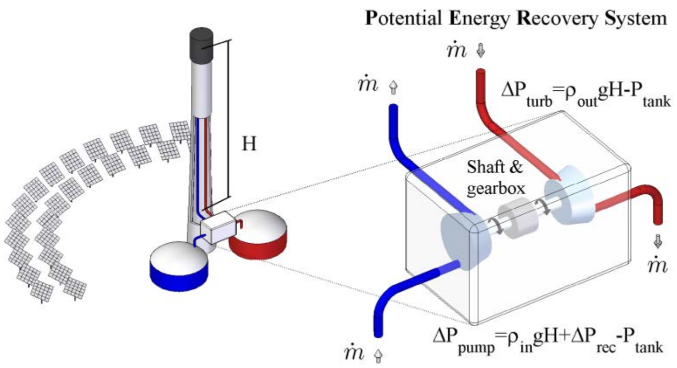

Fig. 1. PERS scheme and location in a solar power tower plant.

The PERS can work in parallel to the traditional dissipative passive system or substitute it. The PERS may be disconnected by a valve if there is the risk of damaging the SPT or if there is low process profitability. A SPT could have more than one PERS operating in parallel.

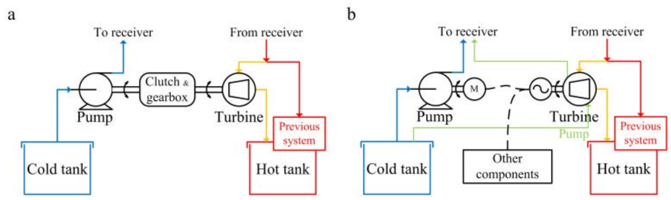

Fig. 2: Block diagram of PERS. a) Mechanical configuration. b) Electrical configuration, [12]**.**

The present study is focused on the mechanical configuration of the PERS [12] , see Figure 2.a. In this configuration, the fluid is conducted through the PERS turbine, transforming the energy of the fluid into mechanical energy. That energy is transmitted through a driving belt, which joins mechanically the PERS turbine with the drive shaft of the feed pump.

The different pump and turbine revolutions can be adjusted using a gear box. Also, a clutch could be installed between pump and turbine to allow the system to engage or disengage, guaranteeing the correct operation in parallel. The mechanical transmission performance between the turbine and the pump is assumed to be 0.98 [13].

Other possibilities of the PERS should not be rejected, for example the electrical configuration, see Figure 2.b. In this configuration the turbine revolutions must be adapted to a generator speed in order to produce electrical energy; that energy could be used by the different components that form the SPT. The energy transformation performance for this configuration is assumed to be 0.85 [13]. In emergency situations this configuration of PERS may reverse the usual operation process. The generator could converse into motor producing enough energy to pump the HTF from the PERS turbine to the receiver, green line of Figure 2.b.

3. Cases studied.

The plants analysed are Gemasolar [14], located in Seville, Spain, which is in operation since 2011; and Crescent Dunes [15], located in Nevada, USA, and currently under construction. Table 1 collects the main parameters of each heliostat field configuration and receiver dimensions.

Crescent Dunes as well as Gemasolar use molten salt as HTF in a cylindrical external receiver. In both plant the solar salt enters into the receiver at 290 ºC and leaves at 565 ºC. However, Crescent Dunes generates four times more electrical power than Gemasolar. It is possible by larger surface of mirrors and receiver, and higher tower. In both cases, the receivers are formed by 16 panels, divided in two flow paths. The receiver efficiencies have been calculated following [4,11].

Table 1. Main design parameters for Crescent Dunes and Gemasolar [11,16–19]**.**

	Crescent Dunes	*Gemasolar*
Latitude [º]	38.24	37.56
Land inclination [º]	0	0
Electricity Generation [GWh/year]	485	110
Number of heliostats	10300	2650
Heliostat width [m]	11.28	10.76
Heliostat height [m]	10.36	10.76
Radius of field boundary [m]	1380	732
North shift of boundary circle [m]	240	179
Tower optical height [m]	180	120
Receiver height [m]	20	10.5
Receiver diameter [m]	17.6	8.5
Receiver panel width [m]	3.5	1.499
Internal tube diameter [m]	0.042	0.033
Number of tubes per panel	76	41
Receiver efficiency	0.76	0.7718

Crescent Dunes and Gemasolar heliostat fields follow a radial staggered arrangement, except in the inner zone of Gemasolar which is cornfield. Based on scaled images the radius of each row has been gathered and along with the number of heliostats per row, both heliostat fields have been generated in Matlab®. Following the methodology by Augsburger [20], only the heliostats inside a boundary circle, whose center is shifted to the north of the tower base, remains in the field. Radius and north shift of boundary circle for the selected fields can be examined in Table 1 and the resulting fields are shown in Figure 3; note the difference in land surface occupied by each field.

The heliostat efficiency, η_{hel}, is the product of loss factors affecting its optical performance [4]:

$$\eta_{hel} = ref \cdot \cos\beta \cdot \eta_{at} \cdot \eta_{s\&b} \cdot \eta_{sp} \quad (1)$$

Where ref is the reflectivity of the mirrors defined as a constant whose value is 0.88 [21]; $\cos\beta$ is the angle between the heliostat normal and the solar radiation direction, which has been computed using the sun position correlation reported in [22]. The atmospheric attenuation losses, η_{at}, depend on the distance of the heliostat and the receiver (S) and are calculated following [23]:

$$\eta_{at} = \begin{cases} 0.99321 - 0.0001176 \cdot S + 1.97 \cdot 10^{-8} \cdot S^2 & S \leq 1000\,\mathrm{m} \\ \exp(-0.0001106 \cdot \mathrm{S}) & S > 1000\,\mathrm{m} \end{cases} \quad (2)$$

The shadowing and blocking factor, $\eta_{s\&b}$, has been computed by means of parallel projection of the neighbor heliostats [24]. Initially fourteen neighbor heliostats are assigned to each heliostat, even though this number is halved neglecting those heliostats behind the plane of the object heliostat.

Finally, the spillage or intercept factor, η_{sp}, is the fraction of reflected solar flux intercepted by the receiver. This factor has been obtained using the methodology described by Sánchez-González [25]. Such method is based in the projection of the flux density distribution from the image plane into the receiver surfaces, considering several aiming points as did Saeb et al. [26]. Further details about flux model for external receiver can be found in [25].

Given a heliostat field composed of N_{hel} heliostats, the hourly efficiency of the field, η_{field}, is:

$$\eta_{field} = \left(\sum_{hel=1}^{N_{hel}} \eta_{hel} \right) \Big/ N_{hel} \quad (3)$$

To avoid a great computational cost in the calculation of the optical efficiency, the methodology proposed by Wagner [27] have been used. Wagner shown that the optimal sample days, equally spaced between the solar declination angle. Thus, the representative Julian day numbers are 172 (summer solstice), 218, 238, 256, 272, 290, 310, and 355 (winter solstice). To calculate the optical efficiency of the field during a whole year, each hourly efficiency has been interpolated from those representative days. This methodology is also used by the free software SAM (Solar Advisor Model) distributed by NREL.

3.1.Field calculation

Firstly, the efficiency of each heliostat for Crescent Dunes and Gemasolar fields has been computed during the sun hours of the 8 representative days. It has been taking into account that the sun hours are different depending on the number of Julian day and on the location of the plant; it means that the sun hours are function of the elevation and azimuthal angles of the sun. A SPT does not work if the sun elevation angle is lower than 15º [28]. Then, the sun hours vary from 6 h to 18 h in summer until from10 h to 14 h in winter.

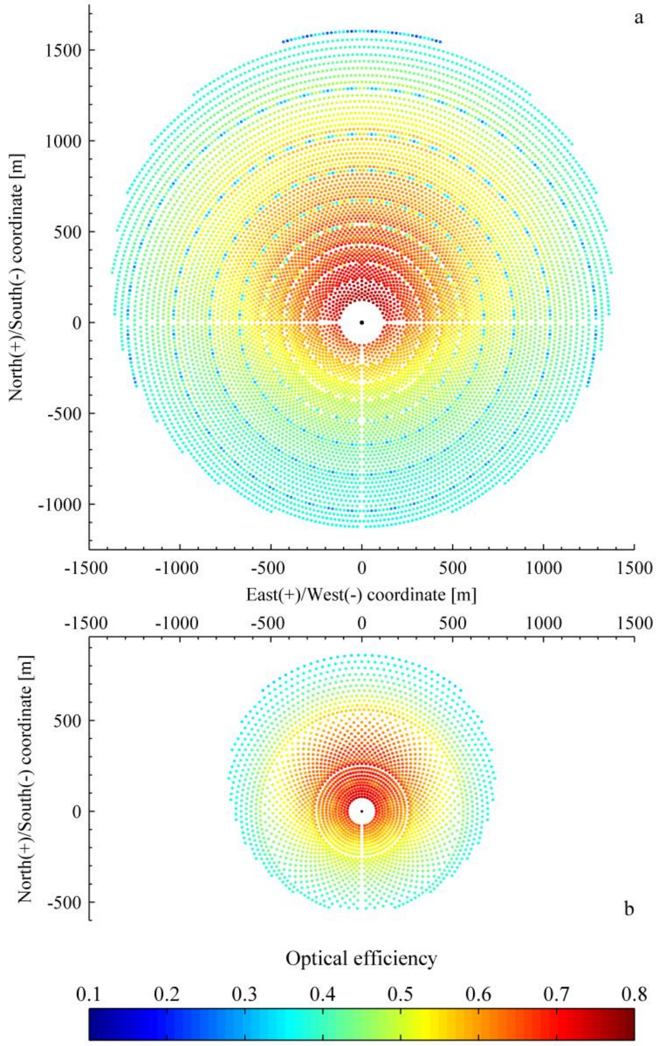

Fig. 3. Heliostat annual average efficiency. a) Crescent Dunes. b) Gemasolar.

For both plants the annual average efficiency of each heliostat has been estimated from the 8 representative days; it is shown in Figure 3. It can be seen that in both fields the heliostats with maximum efficiency are in the north and close to the tower. The range of heliostat efficiencies is similar in either plant. Since, Crescent Dunes has a larger number of heliostats; the field efficiency obtained for Crescent Dunes is lower, as it can be observed in Figure 4 that represents the hourly field efficiency of the 8 representative days. Furthermore, for both plants the efficiency of the field is around 5% higher in summer than in winter.

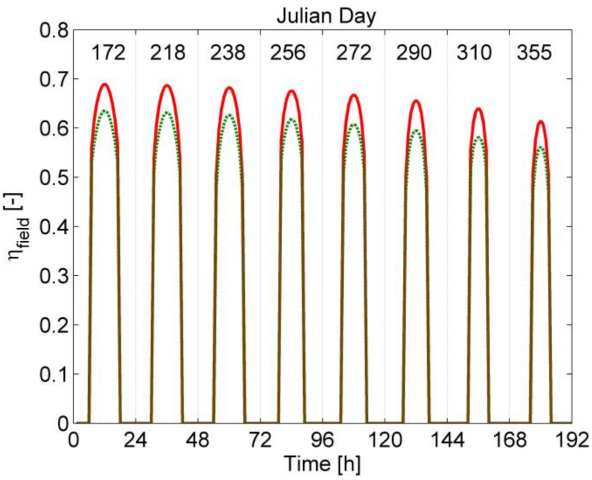

Fig. 4. Hourly efficiency of the heliostat fields for the 8 representative days. Crescent Dunes (dot green line), Gemasolar (solid red line).

4. Energy balance using the PERS.

The feed pump system is compounded by several centrifugal high-pressure vertical pumps working in parallel. In both studied plants the drive system consists of three pumps plus one reserve pump, all them are equal and their operational limit is defined by the maximum mass flow rate at the receiver divided by three.

To calculate the power consumed by the pumping system it is necessary to know the characteristic curves of the pump, given by the manufacturer, and the resistance curve of the system.

To calculate the resistance curve of the system, it is necessary to previously calculate the hourly mass flow rate at the receiver, $\dot{m}_{HTF}$, and the hourly pump head, H .

4.1.Mass flow rate

The hourly mass flow rate is estimated by means of an energy balance between the solar power absorbed by the HTF at the receiver (Equation 4) and the mandatory increase of the temperature of the solar salt at the receiver (Equation 5).

$$E_{HTF} = DNI \eta_{field} N_{hel} A_{hel} \eta_{rec} \qquad (4)$$

$$\dot{m}_{HTF} = \frac{E_{HTF}}{C_p (T_{out} - T_{in})} \qquad (5)$$

Where DNI is the hourly direct normal irradiance obtained from [29], A_{hel} represents the surface of one heliostat, η_{rec} corresponds to the receiver efficiency due to the heat losses, it has been assumed that η_{rec} is constant during the whole year, and its value has been obtained from a previous work [11], T_{in} and T_{out} represent the inlet and outlet temperature of the molten salt at the receiver, 290 ºC and 565 ºC, respectively. C_p corresponds to the specific heat of the salt for an outlet - inlet average temperature obtained from Zavoico [30], and whose value is 1516.5 J/kgK.

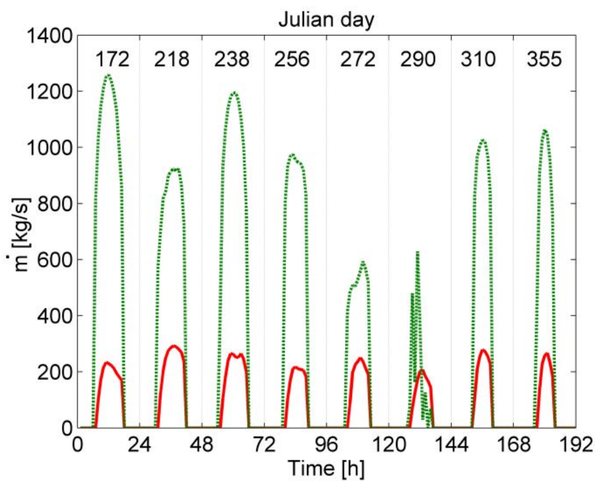

Fig. 5. Mass flow rate for the 8 representative days. Crescent Dunes (dot green line), Gemasolar (solid red line).

Figure 5 shows the mass flow rate variation with time along the 8 representative days, using Equation 5. It can be seen that the mass flow rate in the receiver is strongly dependant on DNI; the chosen data of DNI are a five year prorated data. Therefore, the mass flow rate of the receiver has numerous variations along the year. However, the mass flow rate is higher in summer than in winter. The maximum mass flow rate for Gemasolar is around 335 kg/s (695 m^3/h), while in Crescent Dunes it is four times higher, around 1280 kg/s (2662 m^3/h).

These plants are designed for the maximum mass flow rate obtained. The operation process is as follows: when the mass flow rate is below one third of the maximum flow rate only one pump is working, for medium mass flow rate a second pump also operates, and only when the mass flow rate exceeds two thirds of the design point (maximum mass flow rate) the three pumps work in parallel. In both plants, the solar system operates at least 320 days per year, being the estimated time of operation for one pump at least 3150 hours, for two pumps simultaneously working 2550 hours, and for three pumps simultaneously working 1480 hours in Crescent Dunes, and 2910 hours, 2415 hours, and 1340 hours, respectively, in Gemasolar.

4.2. Pump Head

The head of the pump is defined as the potential power of the tower plus the pressure drop in the receiver and the tower pipes, and minus the pressure in the cold tank. The potential power is a function of the height difference between the cold tank and the receiver, Δh, and of the density of the molten salt at inlet work temperature, $\rho_{HTF,in}$=1906 kg/m^3 [30], while the pressure drop in the receiver has been calculated as Rodriguez-Sanchez et al. [11], considering the receiver a set of straight tubes, elbows, contractions and expansions.

$$\mathrm{H}_{pump} = (\rho_{HTF,in}\, \mathrm{g}\, \Delta h + \Delta p_{\mathrm{rec}} - p_{\mathrm{tank}}) \quad (6)$$

The pressure drop in the receiver, Δp_{rec}, changes with the mass flow rate, therefore it is necessary to modify the operation mode of the pump to obtain the best efficiency as possible. The characteristic equations for a pump with frequency controller are obtained from the similarity relations of the centrifugal pumps. Then, the hourly pump efficiency, η_{pump}, is obtained at the intersection between the characteristic curves of the pump and the resistance curve of the pump system. The estimated hourly power supply by the pump, E_{pump} can be calculated using Equation 7.

$$E_{pump} = \frac{\dot{m}_{HTF} \cdot H_{pump}}{\rho_{HTF,in} \cdot \eta_{pump}} \qquad (7)$$

For this work, Friatec has provided the head, shaft power and efficiency curves of a typical vertical pump used in molten salt SPT, see Figure 6. The model shown is a GVSO pump, whose design point is a head of 330 m, a volume flow rate of 820 m^3/h, and an efficiency of 75.3%. The price of this pump is around 350000 $. The characteristic curves of the pump provided by Friatec are adequate for the operational conditions of Crescent Dunes, see solid lines at Figure 6. However, Gemasolar has been solved using the similarity laws of the centrifugal pumps.

Figure 6 also shows the resistance curve of one feed pump of Crescent Dunes, and it efficiency has been represented by green plus symbols (+). The head of the pump is given by $h_{pump} = 2.9 \cdot 10^{-5} Q^2 + 6.5 \cdot 10^{-3} Q + 343.6$ [m], where Q is the hourly volume flow rate. Although, the efficiency does not follow a perfect second order equation due to the speed control of the pump; several values are shown in Figure 6. To carry out these calculations, it has been assumed smooth tubes and a dynamic viscosity of 0.0016 Pa·s.

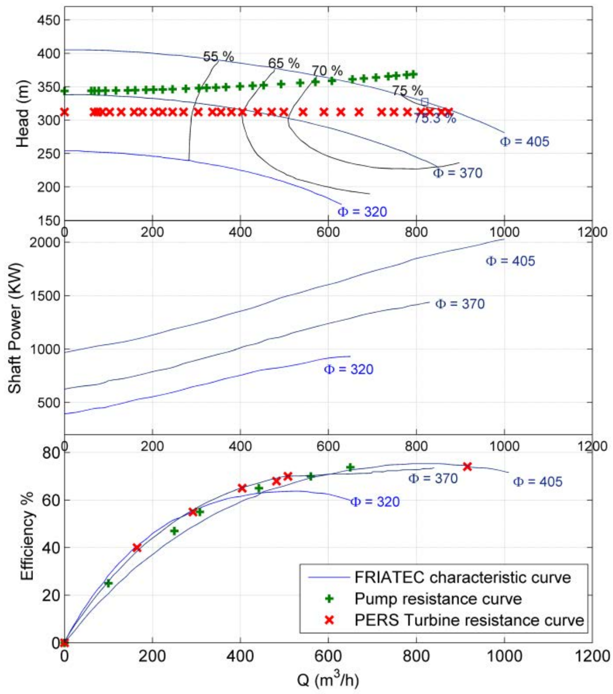

Fig. 6: Characteristic and resistance curves of a GVSO vertical pumps and PERS turbine for Crescent Dunes.

4.3.PERS Turbine

Due to the extreme operational conditions, the PERS turbines must satisfy several requirements: bear high temperatures (about 600 ºC) and a corrosive ambient, high robustness, no moving parts, no lubricant, and no cavities in order to avoid solidification or stagnation. The turbines that could bear these conditions can be the same vertical pumps used to raise the HTF, but operating in turbine regime. The PERS turbine must be installed taking into account the same considerations that the feed pumps. To avoid salt freeze in the starting and stopping it must have a pre-heated system, and it must allow gravity drain.

Nowadays, there is no knowledge of the commercialization of this kind of pumps working as a turbine (PAT). In absence of theoretical and experimental data, the curves of Figure 6 have been used to calculate the efficiency of the turbine, following [31] where is stated that the maximum efficiency is approximately the same in pump and turbine modes. In this case the head of the turbine is constant for the whole range of mass flow rate, and it is equivalent to the height of the column of HTF, $\rho_{HTF,\mathrm{out}} g \Delta h$, where $\rho_{HTF,\mathrm{out}}$ is 1730 kg/m^3 [30]. Then, the power recovered by the turbine can be calculated by Equation 8, where η_{turb} is the instantaneous turbine efficiency calculated with the resistance curve of the turbine and the characteristic curves of the turbine. Note that the volume flow rate at the turbine is higher than at the pump, due to the density variations of the salt.

$$E_{turb} = \eta_{turb} \frac{\dot{m}_{HTF} H_{turb}}{\rho_{HTF,out}} \qquad (8)$$

In Figure 6 a PERS turbine geometrically similar to the feed pump also has been represented by red crosses (x). In addition, to obtain the saved electrical power using the PERS, E_{turb} must be multiplied by the energy transformation coefficients of the corresponding PERS configuration.

4.4. PERS configurations

As a single turbine cannot recover the potential energy of the whole flow rate at the receiver, several PERS configurations have been analysed. Firstly, the possibility of setting up two or three PERS working in parallel has been studied (configurations 1 and 2 of Figure 7). Each turbine is geometrically similar to the feed pumps and between them, and they will be engaged to the corresponding feed pump.

In addition, by similarity other two PERS turbine configurations have been studied. One has a design point equivalent to twice the maximum volume flow rate of the feed pumps (configurations 3 of Figure 7), and the other three times the maximum volume flow rate of the pumps (configurations 4 of Figure 7).

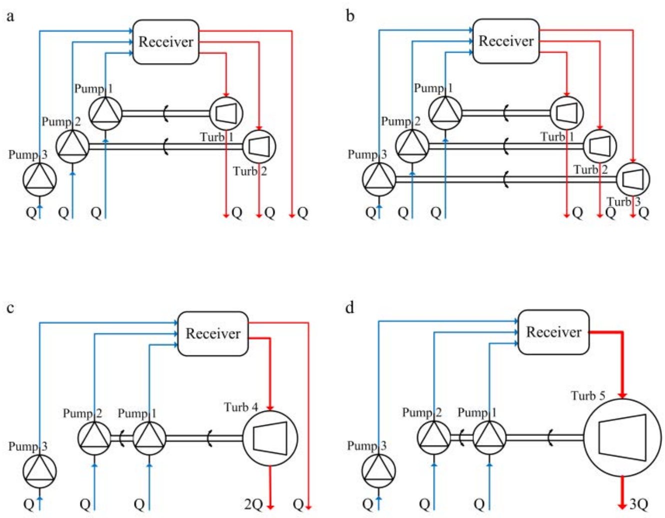

Fig. 7: Different PERS configurations studied. a) Configuration 1: two PERS working in parallel. b) Configuration 2: three PERS working in parallel. c) Configuration 3: One PERS of two times Q_{max}. d) Configuration 4: One PERS of three times Q_{max}.

5. Cost – Benefit analysis.

To complete the PERS implementation study, a cost-benefit analysis (CBA) has been made in order to determinate the income using this system. The model developed by Weibing et al. [32] has been used to calculate the net present value. In addition, the worst scenario described by Perini and Rosasco [33] has been chosen to evaluate the CBA for the PERS.

The benefit of the PERS is equivalent to the profit of the electricity sale and the additional profit resulted from the carbon credits. In the Spanish electrical market around two thirds of the energy is negotiated in a day-ahead spot market. Power plants under special regime may choose once a year between two possible ways of selling their energy: a feed-in tariff or participation in the wholesale market plus a premium [34,35]. Gemasolar is regulated by the feed-in tariff, then this electrical production is paid at 26.93 c€/kWh during the first twenty five years and during the following years the kWh will be paid at 25.4 c€/kWh. The Policy Mechanisms for the CSP electric market in USA are four: power purchase agreement (PPA), renewable portfolio standards that depends of every State, loan guarantee, and investment tax credits [36]. Crescent Dunes has obtained a power purchase agreement with the Nevada Government by which all the energy that the plant will product during the first twenty five years will be acquired at 13.5 c$/kWh [19].

The carbon dioxide released by coal- fired power plants, f, is about 0.9 kg/kWh for USA and 0.93 kg/kWh for Spain [37]. It has been assumed that the price of the coal, P_c, annually increases with constant inflation rate, θ. Then, as the solar electricity sale price is fixed for both studied plants, the annual profit can be expressed as $B^k = E_s P_s^k + fE_s P_c (1+\theta)^{k-1}$, where E_s is the annual electricity output (recovered by the PERS), P_s corresponds to the price of the electricity, and k represents the year of study, from 1 to the whole service period, x, see Table 2.

The cost analysis in the whole service period includes three parts: the principal and interest of loans in the repayment period, the operation and maintenance costs, and the tax costs: $C^k = C_p^k + C_I^k + C_O^k + C_T^k$. It has been assumed that all the investment is borrowed, and that the repayment time is y, see Table 2. An equal principal repayment with interest rate of loan, r, has been used. Note that, the tax cost is only applying to Spain because of in the State of Nevada the societies have fiscal advantages and the income tax rate is zero.

Taking into account the cash flows, and the discount rate τ , it is possible to estimate the total net present value ($TNPV$) and then the profit using the PERS. According to Okoye and Atikol [38] the project is said to be economically feasible if the NPV > 0, if otherwise, it is said to be non-feasible.

$$TNPV = \sum_{k=1}^{n} NPV_k = \sum_{k=1}^{n} \frac{B_k - C_k}{(1+\tau)^k} \quad (9)$$

6. Results.

In this section a study of the best configurations and size of the turbine of the PERS is performed, based on both, energetic and economic analysis.

Figure 8.a shows the sum of the recovered power by each of the three PERS turbines of Crescent Dunes and the relation of this power with the consumption of the feed pumps. It can be seen that the maximum instantaneous power recovered by each turbine is around 1 MW, meanwhile each pump consumed around 3 MW. As the efficiencies are similar for pump and turbine modes, the great difference of power is due to the pressure drop at the receiver, note that the velocity of the salt at the receiver is around 3.8 m/s for the maximum solar flux. In addition, this difference is also caused by the volume flow rate difference at the pump and at the turbine. Note that around one third of the power consumed by the pumps can be recovered reducing the parasitic power consumption of the solar plant. Although the sum of the power recovered by the PERS turbines is always lower than the consumption of the first feed pump, each turbine must be mechanically engaged to the corresponding pump.

For Gemasolar, it has been supposed that the pumps are geometrical similar to the Crescent Dunes pumps for its corresponding flow rate, and relations of similarity for centrifugal pumps have been applied. In addition, it has been assumed that the turbine efficiency increases with the size of the turbine as Equation 10, [39].

$$\frac{1-\eta_{turb,1}}{1-\eta_{turb,2}} = \left(\frac{D_{turb,2}}{D_{turb,1}}\right)^{0.25} \quad (10)$$

Figure 8.b represents the same than Figure 8.a but for Gemasolar. In this case the percentage of recovered power respect to the consumption of the pumps is higher. On one hand, it can be seen in the slope of the pump consumption that the pressure drop at the receiver is lower, due to the velocity of the salt in the tubes of the receiver is around 3.2 m/s for the maximum solar flux. On the other hand, the total volume flow rate of the plant and the tower height are lower, and the pumps consumption lesser, around 2 MW. In this plant, the implementation of PERS can saved around a 50% of the total power consumption of the feed pumps.

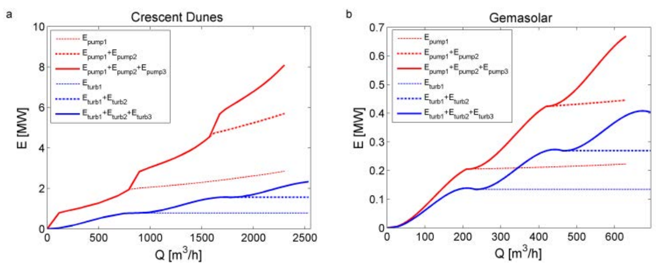

Fig. 8: Power consumed by the feed pumps and power recovered by each of the three PERS turbines working in parallel for Crescent Dunes. a) Individual power. b) Sum of power.

To try to save more energy and taking into account Equation 10 by means the turbine efficiency increases with the size, several turbine sizes have been analysed in order to obtain the optimal PERS design for the analysed plants. Applying the similarity law for turbines other two PERS turbines for each plant have been studied (configurations 3 and 4 of Figure 7).

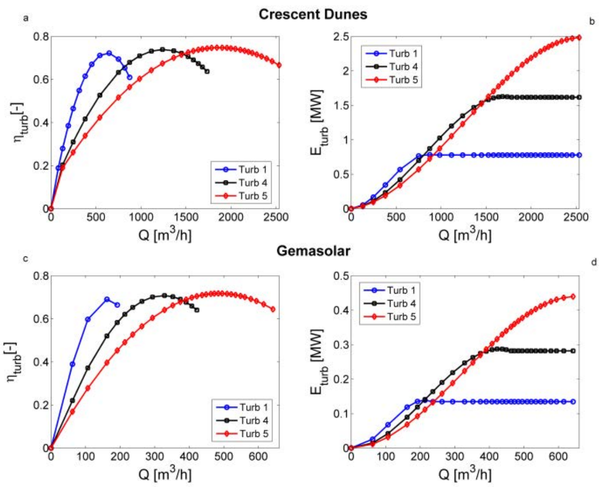

Fig. 9: Geometrical similar turbines for PERS applications. a) Crescent Dunes: Efficiency. b) Crescent Dunes: Power recovered. c) Gemasolar: Efficiency. d) Gemasolar: Power recovered.

In Figures 9.a and 9.c it can be observed that the turbine efficiency grows with the geometrical similar turbine size, from 0.69 for the smallest PERS turbine of Gemasolar to 0.75 for the largest turbine of Crescent Dunes. In addition, the maximum efficiency is displaced to higher flow rates with the turbine size. Figures 9.b and 9.d represent the power recovered by each individual turbine, and as it was expected the largest turbine recover more energy that the others, even more than when three PERS in parallel are used.

A summary of the main results of the PERS implementation in both solar plants is shown in Figure 10. It shows the power recovered by the different configurations of PERS turbines multiplied by the factor of mechanical conversion, the rate of recovered energy respect to the pumps consumption, and the power consumption rate of each of the three pumps of the plants. The power recovered by Crescent Dunes is almost four times higher than the power recovered in Gemasolar. It is due to Crescent Dunes tower is taller than Gemasolar tower and operates with higher flow rate. In addition, the salt velocity in the receiver is higher for Crescent Dunes, producing a larger pressure drop.

The difference in the pressure drop at the receiver increases further the percentage of energy recovered by the PERS in Gemasolar than in Crescent Dunes. It has been estimated that the PERS can recover around 30% of the pump consumption for Crescent Dunes, and 70% for Gemasolar. Overall, the implementation of PERS allows to recover an important part of the power used in pumping the HTF from the tank to the receiver, and then allows to reduce the parasitic power consumption of the plants.

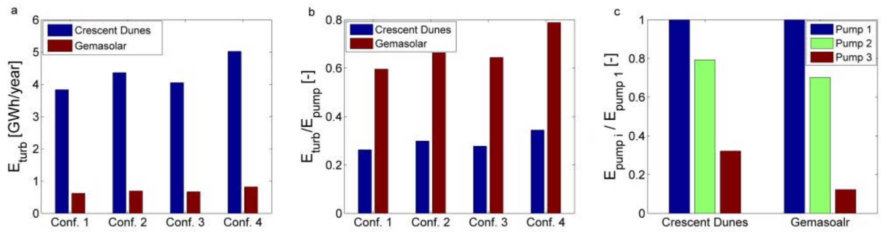

Figure 10. Energy balance results of the PERS implementation in Crescent Dunes and Gemasolar. a) Recovered energy. b) Rate of recovered energy. c) Rate of energy

In Figure 10, it can be seen that the recovered energy by the PERS is similar for configurations 1, 2 and 3. However, in configuration 4 the recovered energy is significantly higher. For the use of turbines of large capacity, it is necessary to compare the recovered power to the power consumed by the pumps, in order to decide if the turbine must be engaged to one, two or the three feed pumps. The power consumed by each of the pumps can be seen in Figure 10.c. For Crescent Dunes the power consumed by the pumps is 16 times higher than for Gemasolar.

In the case of Crescent Dunes the similar turbines (configurations 3 and 4) recover less energy than the energy consumed by the first pump. Then, the PERS turbine must be coupled only to the first pump. However, in Gemasolar the power recovered by configuration 4 is higher than the power consumed by the first pump. Then, its turbine must have a system to couple with the two first pumps, and to decouple of the second pump when it is not working.

In spite of that, an economic analysis is necessary to choose the most adequate PERS configuration, attending not only to energetic considerations but to the economic point of view. To make that decision Table 2 shows the main parameters used for the CBA calculations. For the estimation of the cost of the turbines of larger size than the presented by Friatec the relation of Equation 11 have been used, [40]:

$$C_2 = C_1 \left(\frac{W_2}{W_1} \right)^{0.7} \quad (11)$$

Table 2. Values of economic parameters used in carrying out cost-benefit analysis [32,33].

Economic parameters	***Crescent Dunes***	***Gemasolar***
Inflation rate, θ [%]	3	3
Interest rate of loans, r [%]	**4.18**	**6.77**
Income tax rate, t [%]	0	30
Repayment period of loans, y [year]	10	7
Whole service period, x [year]	30	30
First year maintenance cost, C_O^1 [$]	3000	1500

Solar electricity sale price, P_s [$/kWh]	0.135	0.2693
Carbon dioxide released, f [kg/kWh]	0.9	0.93
Carbon dioxide price, P_c [$/kg]	0.038	0.06
Discount rate, τ [%]	5.5	5.5

The results obtained in the cost-benefit analysis are shown in Figure 11. Although in Nevada the price of the electricity is lower than in Spain the fiscal conditions are better. Adding that the power recovered is higher for Crescent Dunes than for Gemasolar, it can be seen that the economic profit of Crescent Dunes is at least four times higher than for Gemasolar. In spite of that, for both plants the implementation of PERS would be profitable, it has been checked that the flow cash for all the years is positive and that the TNPV is mayor than zero, therefore the project is economically attractive.

Figure 11 shows the average annual cash flow for each studied configuration. As it was expected configuration 4 of PERS has the highest annual cash flow. Configuration 2 is the second more adequate PERS configuration, and Configuration 1 is the worst option.

To finalize with the economic analysis, the payback period has been calculated as the initial investment cost divided by the annual cash inflows. It has been assumed that the total initial investment cost has been paid without bank help. This parameter allows to estimate the time required to recover the cost of the initial investment; longer payback periods are typically not desirable for investment positions. It can be noticed that the first configuration has the shortest payback period and the forth the longer. However, as in all the cases studied the payback period is lower than two years, any configuration could be used.

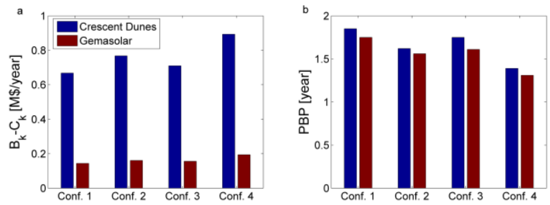

Figure 11. Cost-Benefit analysis. a) Average annual cash flow. b) Payback Period.

7. Conclusions.

The cost reduction and energetic saving using different PERS configurations in two different solar tower power plants have been estimated. The solar plants are located in different countries and one has a power forecast generation 5 times larger than the other. In this way, it is possible to compare the recovered energy between plant sizes and to compare the economic profit between countries.

The PERS configurations analysed are able to recover a significant part of the energy used to pump the HTF thought the receiver. In Crescent Dunes the reduction of the parasitic power consumption of the receiver pumps reaches 26.32% for a turbine of the same size than the feed pump, and up to 34.4% for a geometrical similar turbine of three times the maximum flow rate. While in Gemasolar for the same configurations the recovered energy is 60.57% and 78.84%. This raise in the proportion of the recovered energy is mainly due to the velocity of the HTF in the receiver. The height of the tower plays a minor role in the rate of recovered energy.

However, the net recovered energy is scaled with the size of the plant, (5.02 GWh/year for Crescent Dunes and 0.86 GWh/year for Gemasolar). Therefore, the overall efficiency of the plant improves considerably using the PERS, notably in plants of large power generation capacity and high towers.

Consequently, the profit depends on the plant size and on the market regulation laws of each country. It has been assumed the worst scenario as possible, and in both cases the TNPV is mayor than zero and for every year the annual cash flows are positive. Then, the PERS set-up seems to be a profitable project. In Crescent Dunes for an initial investment cost of 1.26 M$ the average annual cash flow is 0.89 M$/year, and for Gemasolar whose initial investment cost of 0.26 M$ the average annual cash flow is 0.19 M$/year. In addition, the payback period is always lower than two years.

Finally, the optimal PERS configuration would be the set-up of only one turbine of a design point three times the design flow rate of one feed pump. The second best option would be the implementation of three parallel turbines of the same size that the feed pumps.

Acknowledgements.

The authors would like to thank to Friatec by the pumps data and curves provided. The financial support from CDTI and S2m Solutions for the MOSARELA project (Molten salt receiver lab), whose reference is IDI-20120128. Finally, the financial support of the ENE2012-34255 project is also acknowledged.

Bibliography.

[1] Blanco J, Heller P, Mehos M, Meier A, Meyer R. Solar Power and Chemical Energy Systems Annual Report. 2010.

[2] Hoffschmidt B, Alexopoulos S, Göttsche J, Sauerborn M, Kaufhold O. Comprehensive Renewable Energy. Elsevier; 2012.

[3] Keith Lovegrove, Muriel Watt, Robert Passey, Graeme Pollock, Joe Wyder JD. Realising the Potential of Concentrating Solar Power in Australia. itp; 2012.

[4] Benammar S, Khellaf a., Mohammedi K. Contribution to the modeling and simulation of solar power tower plants using energy analysis. Energy Convers Manag 2014;78:923–30.

[5] Jianfeng L, Jing D, Jianping Y. Heat transfer performance of an external receiver pipe under unilateral concentrated solar radiation. Sol Energy 2010;84:1879–87.

[6] Lata JM, Rodrí uez M, de Lara MA. High Flux Central Receivers of Molten Salts for the New Generation of Commercial Stand-Alone Solar Power Plants. J Sol Energy Eng 2008;130:021002:1–5.

[7] Yang X, Yang X, Ding J, Shao Y, Fan H. Numerical simulation study on the heat transfer characteristics of the tube receiver of the solar thermal power tower. Appl Energy 2012;90:142–7.

[8] Huang W, Xu Q. Development of an analytical method and its quick algorithm to calculate the solar energy collected by a heliostat field in a year. Energy Convers Manag 2014;83:110–8.

[9] McGovern RK, Smith WJ. Optimal concentration and temperatures of solar thermal power plants. Energy Convers Manag 2012;60:226–32.

[10] Kolb GJ, Ho CK, Mancini TR, Gary JA. Power Tower Technology Roadmap and Cost Reduction Plan. Alburquerque: 2011.

[11] Rodríguez-Sánchez MR, Soria-Verdugo A, Almendros-Ibáñez JA, Acosta-Iborra A, Santana D. Thermal design guidelines of solar power towers. Appl Therm Eng 2014;63:428–38.

[12] Santana D, Wiesenberg R, Serrano E, Villa J. Solar Power Tower System. 13/246, 496, 2011.

[13] Tenerelli J. Efficiency of the energy conversion. College of Earth and Mineral Sciences; n.d.

[14] Torresol Energy: Gemasolar. http://www.torresolenergy.com/TORRESOL/gemasolar-Plant/en 2010.

[15] SolarReserve: Crescent Dunes. Http://www.solarreserve.com/what-We-Do/csp-Projects/crescent-Dunes/ 2014.

[16] Trabish HK. A Climb Up the SolarReserve Solar Power Tower. http://www.greentechmedia.com/articles/read/A-Climb-Up-the-SolarReserve-Solar-Power-Tower 2013.

[17] Burgaleta JI, Arias S, Ramirez D. Gemasolar, the first tower thermosolar commercial plant with molten salt storage. Solarpaces, 2011, p. 1–8.

[18] Lata J, Alcalde S, Fernández D, Lekube X. First surrounding field of heliostats in the world for commercial solar power plants - Gemasolar. In: Sener, editor. Solarpaces, 2010, p. 1–9.

[19] NREL: National Renewable Energy Laboratory. Http://www.nrel.gov/csp/solarpaces/by_project.cfm 2011.

[20] Augsburger G. Thermo-economic optimisation of large solar tower power plants. EPFL, 2013.

[21] Noone CJ, Torrilhon M, Mitsos A. Heliostat field optimization: A new computationally efficient model and biomimetic layout. Sol Energy 2012;86:792–803.

[22] Duffie JA, Beckman WA. Solar engineering of thermal processes. New York: Wiley; 1991.

[23] Schmitz M, Schwarzbözl P, Buck R, Pitz-Paal R. Assessment of the potential improvement due to multiple apertures in central receiver systems with secondary concentrators. Sol Energy 2006;80:111–20.

[24] Collado FJ, Guallar J. Campo: Generation of regular heliostat fields. Renew Energy 2012;46:49–59.

[25] Sánchez-González A, Santana D. Solar flux distribution on central receivers: a projection method from analytic function. Renew Energy 2014;Submitted.

[26] Besarati SM, Yogi Goswami D, Stefanakos EK. Optimal heliostat aiming strategy for uniform distribution of heat flux on the receiver of a solar power tower plant. Energy Convers Manag 2014;84:234–43.

[27] Wagner MJ. Simulation and Predictive Performance Modeling of Utility-Scale Central Receiver System Power Plants. University of Wisconsin, Madison, 2008.

[28] Collado FJ, Guallar J. A review of optimized design layouts for solar power tower plants with campo code. Renew Sustain Energy Rev 2013;20:142–54.

[29] US Department of Energy. EnergyPlus Energy Simulation Software. http://apps1.eere.energy.gov/buildings/energyplus/energyplus_about.cfm 2013.

[30] Zavoico AB. Solar Power Tower: Design Basis Document. San Francisco: 2001.

[31] Derakhshan S, Nourbakhsh A. Experimental study of characteristic curves of centrifugal pumps working as turbines in different specific speeds. Exp Therm Fluid Sci 2008;32:800–7.

[32] Li W, Wei P, Zhou X. A cost-benefit analysis of power generation from commercial reinforced concrete solar chimney power plant. Energy Convers Manag 2014;79:104–13.

[33] Perini K, Rosasco P. Cost–benefit analysis for green façades and living wall systems. Build Environ 2013;70:110–21.

[34] Spain Government. Real Decreto 436/2004, de 12 de marzo. Spain: 2007.

[35] Usaola J. Participation of CSP plants in the reserve markets: A new challenge for regulators. Energy Policy 2012;49:562–71.

[36] Gallego B, Bial M. CSP Global MARKETS. 2013.

[37] International Energy Agency. CO2 emissions from fuel combustion. 2012.

[38] Okoye CO, Atikol U. A parametric study on the feasibility of solar chimney power plants in North Cyprus conditions. Energy Convers Manag 2014;80:178–87.

[39] Dixon SL, Hall CA. Fluid Mechanics and Thermodynamics of Turbomachinery. 7th editio. Butterworth Heinemann; 2014.

[40] Towler G, Sinnott RK. Chemical Engineering Design. Second. Elsevier; 2013.

List of Figures

Fig. 1. PERS scheme and location in a solar power tower plant.

Fig. 2: Block diagram of PERS. a) mechanical configuration. b) electrical configuration, [12].

Fig. 3. Heliostat annual average efficiency. a) Crescent Dunes. b) Gemasolar.

Fig. 4. Hourly efficiency of the heliostat fields for the 8 representative days. Crescent Dunes (dot green line), Gemasolar (solid red line).

Fig. 5. Mass flow rate for the 8 representative days. Crescent Dunes (dot green line), Gemasolar (solid red line).

Fig. 6. Characteristic and resistance curves of a GVSO vertical pumps and PERS turbine for Crescent Dunes.

Fig. 7. Different PERS configurations studied. a) Configuration 1: two PERS working in parallel. b) Configuration 2: three PERS working in parallel. c) Configuration 3: One PERS of two times Qmax. d) Configuration 3: One PERS of three times Qmax.

Fig. 8. Power consumed by the feed pumps and power recovered by each of the three PERS turbines working in parallel for Crescent Dunes. a) Individual power. b) Sum of power.

Fig. 9. Geometrical similar turbines for PERS applications. a) Crescent Dunes: Efficiency. b) Crescent Dunes: Power recovered. c) Gemasolar: Efficiency. d) Gemasolar: Power recovered.

Figure 10. Energy balance results of the PERS implementation in Crescent Dunes and Gemasolar. a) Recovered energy. b) Rate of recovered energy. c) Rate of energy

Figure 11. Cost-Benefit analysis. a) Average annual cash flow. b) Payback Period.

List of Tables

Table 1. Main design parameters for Crescent Dunes and Gemasolar [6,13–16 , estimations].

Table 2. Values of economic parameters used in carrying out cost-benefit analysis [32,33].